Acoustic characterization of a miniature matrix transducer for pediatric 3D transesophageal echocardiography

Daeichin, Verya; Bera, Deep; Raghunathan, Shreyas; Shabani Motlagh, Maysam; Chen, Zhao; Chen, Chao; Noothout, Emile; Vos, Hendrik J.; Pertijs, Michiel; de Jong, Nico

Acoustic characterization of a miniature matrix transducer for pediatric 3D transesophageal echocardiography

Verya Daeichin[*, *]

v.daeichin@tudelft.nl

Deep Bera[†]

Shreyas Raghunathan[*]

Maysam Shabani Motlagh[*]

Zhao Chen[‡]

Chao Chen[‡]

Emile Noothout[*]

Hendrik J. Vos[*, †]

Michiel Pertijs[‡]

Johan G. Bosch[†]

Nico de Jong[*, †]

Martin Verweij[*, †]

[*]Lab. of Acoustical Wavefield Imaging, Delft University of Technology, Delft, The Netherlands

[†]Dept. of Biomedical Engineering, Thoraxcenter, Erasmus MC, Rotterdam, The Netherlands

[‡]Electron. Instrum. Lab., Delft University of Technology, Delft, The Netherlands

[*]Address correspondence to: Verya Daeichin, Ph.D., TU Delft, Imphys / Acoustical Wavefield Imaging, Lorentzweg 1, 2628 CJ Delft. Phone: +31(0)15 2782025.

Abstract

This paper presents the design, fabrication and characterization of a miniature PZT-on-CMOS matrix transducer for real-time pediatric 3-dimensional (3D) transesophageal echocardiography (TEE). This 3D TEE probe consists of a 32 × 32 array of PZT elements integrated on top of an Application Specific Integrated Circuit (ASIC). We propose a partitioned transmit/receive array architecture wherein the 8 × 8 transmitter elements, located at the centre of the array, are directly wired out and the remaining receive elements are grouped into 96 sub-arrays of 3 × 3 elements. The echoes received by these sub-groups are locally processed by micro-beamformer circuits in the ASIC that allow pre-steering up to ±37°. The PZT-on-CMOS matrix transducer has been characterized acoustically and has a centre frequency of 5.8MHz, -6dB bandwidth of 67%, a transmit efficiency of 6kPa/V at 30mm, and a receive dynamic range of 85dB with minimum and maximum detectable pressures of 5 Pa and 84 kPa respectively. The properties are very suitable for a miniature pediatric real-time 3D TEE probe.

Key Words: Transesophageal echocardiography; pediatric matrix transducer; ASIC; volumetric imaging; micro-beamforming

Introduction

Transesophageal echocardiography (TEE) concerns ultrasound imaging of the heart from the esophagus with an ultrasound transducer mounted on the tip of a gastroscopic tube (Seward, et al. 1988). Since the introduction of

TEE transducers in the 1980s (Pandian, et al. 1992, Roelandt, et al. 1992), this imaging modality has been widely used for diagnosis and real-time intra-operative imaging of the heart to guide minimally invasive cardiac procedures (Kwak, et al. 2010). Often, 2-dimensional (2D) TEE is used for monitoring and the final check at the end of the operation. However, such 2D cross-sectional visualization of the heart is insufficient in the case of complicated reconstructions since the imaged targets (cardiac and valve anatomy, motion, blood flow etc.) are all 3-dimensional (3D) phenomena and hard to be interpreted from only 2D cross-sections. Recent advances in 2D matrix array technology (Christiansen, et al. 2015, Light, et al. 2001) have allowed the real-time 3D reconstruction of the cardiac anatomy by TEE. Various publications have shown the advantages of 3D echocardiography over 2D, both for TEE and transthoracic imaging (TTE) (Gopal, et al. 1994, Handke, et al. 2002, Provost, et al. 2014, Raichlen, et al. 1986, Salustri, et al. 1995, Sapin, et al. 1993, Sugeng, et al. 2003).

Implementation of imaging sequences for 3D imaging ideally requires access to every individual element of the 2D array so that transmit and receive timing and apodization can be controlled for each element. However, given the desired aperture of a 2D array, the need for keeping the pitch between the elements less than half the wavelength results in thousands of elements. Directly connecting every individual element to an ultrasound unit (with up to a few hundred channels) is impractical if not impossible. As an example, a TEE probe with aperture size of 9×9 mm^2 and a central frequency of 5MHz (wavelength of about 300 µm) requires a $60 \times 60 = 3600$ element array. The data transfer rate for all individual elements would amount to terabits per second.

Several solutions have been proposed to solve this problem. To reduce the cable and channel counts, some have proposed to group the elements of a 2D array into column and row configurations (Chen, et al. 2014, Christiansen, et al. 2015, Logan, et al. 2011) or to use multiplexing techniques (Savord and Solomon 2003, Shell 2002). Both methods have the limitation of not allowing continuous access to the full array during transmission and reception since only part of the elements is connected to the scanner at a given time. A more direct solution for reducing the cable or channel counts is based on sparsity: only a sparse subset of the elements are connected, instead of the full array (Austeng and Holm 2002, Diarra, et al., Provost, et al. 2014, Roux, et al. 2017, Roux, et al. 2016). Although this is a promising technique, it requires more complex sequences and beamforming algorithms and the element configuration in a sparse array must be optimized to achieve acceptable image quality in terms of resolution and contrast to noise ratio.

Perhaps the most elegant way to achieve data reduction is the micro-beamforming (or sub-array beamforming) technique, which greatly reduces the number of required cables and the data transfer rate for such an array (Chen, et al. 2017, Chen, et al. 2016, Chen, et al. 2014, Fisher, et al. 2005, Kortbek, et al. 2013, Matrone, et al. 2014, Wygant, et al. 2009). This technique performs the first step of the beamforming already in the probe tip using an application specific integrated circuit (ASIC). Per sub-array, partial beamforming is performed by applying micro-delays to the signal of each element and summing all signals.

Several TEE probes with matrix array transducers have been developed. Currently, there are three commercially available 3D TEE probes: X7-2t (Philips Ultrasound, Bothell, WA), Vivid E9 BT12 (General Electric Healthcare, Amersham, U.K.), and Siemens Acuson SC200 Z6M (Siemens Healthcare GmbH, Munich, Germany). However, there is no published report on characterization and technology of either of these TEE probes. The big size of these probes (2-3 cm^3) is limiting the use of such a 3D TEE technology on pediatric patients as well as for long intra-operative monitoring in adult patients. To overcome this, significant reduction in the size of the probe head is required. We have developed a matrix transducer using micro-beamforming and ASIC technologies for TEE application which can be accommodated in a head smaller than 1 cm^3. In this paper wediscuss the design, technical aspects, acoustic characterization and performance of our miniaturized matrix transducer for a TEE probe. To the best of our knowledge this is the first report to discuss the details of such probe.

Materials and Methods
Requirements and initial design choice

The requirements for a miniature TEE probe are more challenging than those for its adult (Blaak, et al. 2011) and have been described in an earlier publication (Chen, et al. 2017, Chen, et al. 2016). The physical constraints include a head volume of not more than 1 cm^3, and less than 200 individual cables in the shaft of 5mm in diameter. The head volume limits the aperture area of the transducer array to 5 mm × 5mm. The intended penetration depth is up to 12cm and the central frequency around 5MHz. Thus for this central frequency of 5MHz, the pitch of the 2D PZT array is chosen as $\lambda/2$ (150 µm) in both directions to minimize grating lobes (Cobbold 2006). Thus, within the 5 mm × 5mm aperture area we fabricate $32 \times 32 = 1024$ individual PZT elements. The dicing kerf between the elements is 20 µm.

Within the available aperture of 25 mm^2, and the1024 total number of squared elements, different partitioned designs with separated transmitters and receivers have been evaluated numerically. In our design, we chose to partition the aperture into a small set of transmit elements and sub-arrays of receive elements that are connected to the ASIC for micro-beamforming. The transmit elements are electrically fully separated from the receive electronics and directly wired out to the ultrasound system, allowing full freedom of choice of transmit signals (AWG pulse shapes, delays, voltages, coding, and etc.). This still leaves us the choice of the location of the transmit elements. We considered three different designs with a cross shaped transmitter, a central transmitter and staggered transmitter elements. These three architectures are evaluated by simulations based on multiple quality parameters such as width of the transmit beam, lateral and elevational resolution of the receiver and grating lobe and side lobe levels. Simulations for the transmit and receive beam profiles were carried out using Field II (Jensen 1996) using the transducer element transfer function obtained from PZ-Flex simulations. A three cycle Gaussian modulated pulse was used as the excitation function for the array. In all the designs, a transducer element designated as a transmitter is incapable of acting as a receiver and vice versa. Therefore, the transmitter elements appear as missing element in the receive aperture.

Pre-beamforming and ASIC design

The 32 × 32 array elements are directly connected to a matrix of spatially coaligned contacts on the ASIC using an interconnect layer (Chen, et al. 2017, Chen, et al. 2016). The ASIC (thickness 300 μm) has been fabricated in low-voltage CMOS technology, which is only possible because of the partitioned design where high voltage transmit elements are wired out directly to the mainframe, while only the signals from receive elements are routed into the ASIC for pre-processing. As said, to reduce the number of output signal channels, the sub-array beamforming method, also referred to as "micro-beamforming" or "pre-steering", is adopted in this work (Yu 2012). In this case, the transducer matrix is divided into sub-arrays of 3 × 3 elements, the receive signals of which are delayed and summed by the local micro-beamformer circuit in the ASIC, reducing the number of channels by a factor of 9. In the micro-beamformer, fine delays are applied to the individual elements, so that the sub-array is acting as a large element pre-steered roughly into a predefined direction. The micro-beamforming circuit is based on a sample-and-hold delay line and charge-domain summation providing a delay resolution of 30ns and a delay depth of 180ns to steer the beam in both azimuthal and elevation directions over ±37°. The signals of all sub-arrays are further beamformed in the imaging system that applies larger delays to perform the full-aperture beamforming, steering and focusing. All components in the ASIC (LNAs, micro-beamformers, line drivers, logic etc) are designed for minimal power consumption to avoid overheating of the probe tip. The expected power consumption for a 96 receiver subgroups is about 230 mW (270 μW/element). The front-end signal conditioning in each channel is performed by the LNA and a time-gain-compensation (TGC) amplifier. The LNA provides 3 gain settings (-12dB, 6dB and 24 dB) followed by the 4-step TGC gain settings (0dB, 6dB, 12dB and 18 dB). Combining the gain settings of the LNA and TGC results in a gain range of -12 to 42dB assuring a large dynamic range for receiving the echo signals.

Design of single transducer element

A single acoustic transducer was simulated and optimized using PZFlex, a finite difference analysis software package (Abboud, et al. 1993). Commercially available CTS 3203HD is used as the piezoceramic material with a matching layer (conductive glue) mounted on top of a CMOS chip and connected via an interconnect backlayer. The material properties of different materials used in this scheme are given in Table 1. For the intended centre frequency for this 3D TEE probe of 5MHz, a piezoceramic thickness of 225 μm was chosen. In order to optimize thicknesses of the layers, simulations were performed for all different matching and backing layer thicknesses from 40 μm to 140 μm in steps of 10 μm. Thus, 11 × 11 = 121 corresponding FDM simulations were performed using PZFlex and hence the performance of 121 different acoustic stacks was compared in terms of electrical impedance and acoustic pressure at the surface of the transducer.

Table1 Material properties used in FDM simulation

alt-text: Table1

Material	Properties
Conductive Glue	ρ = 3350kg/m3, cp = 2000m/s, cs = 1050 m/s
CTS 3203 HD	c11 = c22 = 137, c12 = 88, c13 = c23 = 92, c33 = 126, c44 = c55 = 22, c66 = 25MPa e15 = e24 = 16, e31 = e32 = 9, e33 = 22C/m2 ε11 = ε22 = 1306, ε33 = 1200CV/m.
Epoxy	ρ = 2975kg/m3, cp = 1960m/s, cs = 1047 m/s
Silicon	ρ = 2330kg/m3, cp = 7526m/s, cs = 4346 m/s

Fabrication of the matrix TEE prototype

Given the specification and the initial design choices, a 32 × 32 array was fabricated. In this work, we have extended the PZT-on-CMOS integration scheme that was used in our previous work (Chen, et al. 2016). Gold balls are applied on top of the ASIC's transducer bond-pads, arranged as a 32 × 32 matrix with a pitch of 150 μm at the surface of the ASIC's metallic interconnect layers. A non-conductive epoxy is deposited between the balls to electrically isolate them, and is ground down to expose the gold, forming electrical contact points for the PZT matrix. Besides functioning as electrical isolation, the non-conductive epoxy also acts as a mechanical dicing buffer (buffer layer, 30 μm thickness). On top of the epoxy, we mount the acoustic stack, which consists of an electrically conductive epoxy glue of 60 μm thickness on both sides of the 225 μm thick CTS 3203HD piezoceramic. The electrically conductive glue provides the electrical connection between the PZT and the exposed metal interconnects on the ASIC and together with the buffer layer act as a backing layer. The acoustic stack is then diced using a 20 μm dicing saw to create 32 × 32 individual PZT transducers. For the purpose of electrical separation, the dicing kerfs extend into the buffer layer for about 10 μm. An aluminium ground foil (8 μm) is glued to the matching layer, on top of the PZT. The total thickness of the assemble transducer is 683 μm.

Acoustic characterization

The 32 × 32 PZT-on-CMOS array was mounted on a PCB daughter-board which was connected to a motherboard that interfaces to a Verasonics (Vantage System, Verasonics Inc. Kirkland, Washington, USA) data acquisition system. The motherboard is designed such that it can be mounted on the Verasonics machine using two Cannon connectors (LLC DLM5-260PW6A, ITT corporation, NY, USA). Commercially available micro-coaxial cables (Samtec, New Albany, IN, USA) are used to transfer the TX(64) and RX(96) data between the daughterboard and the motherboard. The signals from the receive part of the system are recorded using one of the two connectors of the Verasonics system, while the high-voltage transmit signals are provided to the transmit array via the other. The 8 × 8 transmit array elements are directly wired out of the ASIC (via the metallic interconnect top layers of the ASIC, without connection to the electronics) and connected via the motherboard to the Verasonics or other pulsers for acoustical tests. The receive elements are connected to the electronic circuitry in the ASIC via the metal interconnects. The signals from 3 × 3 elements are micro-beamformed, amplified and passed to the cable drivers in the PCB and recorded using the Verasonics. In this paper, the results from the acoustical performance are discussed in detail. The detailed evaluation of the electronics can be found in (Chen, et al. 2017). The prototype was immersed in a water tank for acoustic characterization and the 8 × 8 transmitter and the 96 sub-groups of the receiver were evaluated separately.

To measure the variation in sensitivity between the individual elements (transmitters) and individual sub-groups (receivers) the entire array was used in receive mode and was exposed to a pseudo-planar wave (see supplementary Figure 1) emitted by an external 5MHz 0.5-inch single-element transmit transducer (V309, Olympus Scientific Solutions, Waltham, MA, USA) at a distance of 32cm transmitting a 3-cycle burst with an input peak-to-peak voltage of 10V. The variation in sensitivity of the individual 64 elements of the transmit array was then measured by using them in receive mode and calculating the variation of the amplitude of the received signals. The same approach was used for determining the sensitivity variation of the 96 receive sub-groups.

In order to evaluate the frequency response of a single element of the array, three single elements of the transmit array were chosen randomly and excited by a short (10 ns) pulse with an input peak-to-peak voltage of 20V using an arbitrary waveform generator (33250A, Keysight Technologies, Santa Clara, CA, USA). The generated acoustic signal was recorded at 15mm away from the transducer surface with a 0.2mm needle hydrophone (Precision Acoustics, Dorchester, U.K.). The signals were compensated for the excitation pulse and the hydrophone transfer function before determining the transfer function of the three single elements.

The efficiency of the transmit elements was measured by exciting the entire transmit sub-array (64 elements) with a 3-cycle 5MHz pulse from the Verasonics and varying the excitation voltage from 10V to 40V. The generated pressure waves were recorded using the needle hydrophone on axis in the far field (30mm from the transducer surface). Peak-to-peak pressures generated by the transmit array as a function of peak-to-peak input voltages were recorded and the signals were corrected for the attenuation in water.

The pulse echo measurements were carried out by coupling the prototype with acoustic gel to a quartz plate at a distance of 5mm from the transducer surface. All the transmitters were excited simultaneously with a 3-cycle 5MHz burst of 2V using the Verasonics. The LNA and TGC gains of the receive groups in the ASIC were both set to the moderate gain of 6dB, amplifying the echo signals by a total gain of 12dB before recording by the Verasonics input channels. A constant Verasonics TGC setting of 500 was used to avoid saturation and clipping of the receive signals.

The dynamic range of the receiver, i.e. the largest range of pressures which can be detected by the transducer, was measured as follows. The external 5MHz single-element transducer was excited with a 3-cycle burst of varying voltage to generate a pressure range of 0.2 Pa to 300 kPa at the surface of the prototype placed 32cm away from the source. The corresponding micro-beamformer output was recorded by the Verasonics for three different gain settings of the ASIC signal conditioning circuit. The highest LNA and TGC gain settings of 24dB and 18dB (42dB in total) were used for recording the lower range of the pressures. For the middle range, the gain settings were 6dB and 6dB (12dB in total). For the higher range, LNA gain of -12dB and TGC gain of 0dB (-12dB in total) were used. The signals recorded by the Verasonics were band pass filtered (cut-off frequencies of 4 and 6 MHz) using a 5th order Butterworth filter in MATLAB. Then, the peak-to-peak amplitudes of the received signals (no averaging) were plotted against the input pressure at the transducer surface. To calculate the minimum and maximum detectable pressures from the plot, linear curves were fit to three different parts of the dataset: the noise part (input pressures up to 2 Pa), the linear part (input pressures from 10 Pa to 10 kPa), and the saturated part (above 200 kPa). The intersection of the linear part with the noise part and the saturated part were chosen as the minimum and the maximum detectable pressures respectively.

Furthermore, the transmit-receive beam profile at three different steering angles ((0°,0°), (17°,17°), and (37°,37°)) was evaluated. The beam-profile of the transmit array was determined by mounting the hydrophone on the X-Y stage of the water tank and performing a linear scan in the lateral and elevation directions for each steering settings at 15mm from the surface of the transducer. The different elements of the transmitter were driven by a 3-cycle 5MHz pulse from the Verasonics with different time delays, in order to achieve a transmit steering of (0°,0°), (17°,17°), and (37°,37°). The peak-to-peak pressure recorded by the hydrophone was then recorded for different hydrophone positions for all steering angles and corrected for the hydrophone directivity (see supplementary material and supplementary Figure 2). For the receive beam-profile the prototype was mounted on a rotational arm in the water-tank, in front of the single-element 5MHz transducer driven by a 3-cycle 5MHz burst. In order to construct echoes from different angles, the prototype was rotated from -50° to +50° in steps of 2° laterally with respect to the source. The acoustic signal from the 96 sub-arrays was captured at every angle using the Verasonics and the beam-profile of the individual sub-groups was computed. Using the appropriate delays with respect to the centre of the sub-groups, the beam-profile of the entire receive array was calculated from the data acquired by all the sub-groups at all the angles. The elevation beam-profile of the sub-groups and the receive array was measured by re-positioning the prototype 90 degrees rotated with respect to the previous configuration such that the rotational arm of the water-tank now records the elevation beam-profile. The receive ASIC is capable of providing delays from 30ns to 210ns in steps of 30ns to

each receive element within the sub-group. Thus, in line with the findings in (Yu 2012), we can steer the individual sub-groups to angles 0°, ±17°, and ±37° along the lateral and elevation directions. The net transmit-receive beam profile is described by the product of the transmit and receive angular responses. Therefore, after calculating the transmit and receive beam profile at these three different angles, the beams were combined using the product of transmit and receive beams in both lateral and elevation directions at each angle to acquire the overall transmit-receive beam profiles for steering angles of (0°,0°), (17°,17°), and (37°,37°).

3D imaging

To demonstrate the 3D imaging capability of the prototype, a pattern of five point scatterers (steel balls on needles), forming a rotated letter "T", was placed at a distance of approximately 40mm in front of the transducer array. The sub-arrays were presteered in each of the 25 possible directions. Diverging waves were transmitted from the transmit sub-array in matching directions, using pulses of 18 Vpp (Volt peak-to-peak), generated by the Verasonics system. A 3D volume image was reconstructed by combining the sub-group output signals recorded using the Verasonics system from multiple of such transmit–receive events and rendered to get a frontal view of the point scatterers. The details of the transmit-receive configuration as well as the 3D beamforming algorithm can be found in (Bera, et al. 2016). The 3D image reconstruction has been done offline and 169 transmit-receive events were used to generate one volume.

Results

In the previous sections, we described the design optimisation and manufacturing processes of the acoustic stack for optimal transmission and receive properties of a single transducer element. In this section, we present the result of our simulated model and the experimental results acquired with our prototype matrix TEE transducer for a transmit-receive architecture capable of attaining 3D ultrasound images.

Design choice

From the numerical study, we found that an optimized transducer would have a backing layer thickness of around 90 μm and matching layer thickness of around 70 μm. Given these parameters, we obtain a centre frequency of around 5.5MHz, a bandwidth of 70% and a transmit efficiency of 8.4kPa/V at 30mm for 64 transmit elements and a Johnson-Nyquist noise voltage equivalent of around 8 nV $/\sqrt{Hz}$ for an operating temperature of 37° C and 70% bandwidth.

Three different transmitter architectures were simulated in Field II and their beam profiles were analysed. The different designs and their corresponding beam profiles are shown in Figure 1. The green blocks in the Figures denote the receiver elements of the array and the white spaces denote the transmitter positions.
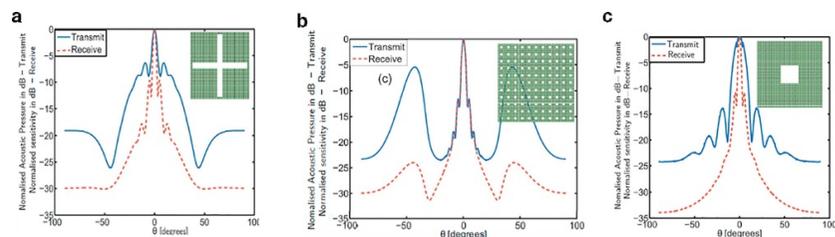

Fig.1 Architecture and transmit and receive beam profiles for a) a cross shaped transmitter; b) a staggered transmitter; c) a central transmitter.

alt-text: Fig 1

To generate sufficient acoustic power the entire transmit array should be excited. Accordingly, the design with the central transmitter (Figure 1c) benefits from a larger opening angle of 13.2 degrees (-3dB points) in comparison to 3.2 degrees with the other two designs (Figure 1a and 1b). A symmetric broad beam with reasonable power generated by the central transmitters can illuminate a larger area with a single excitation, allowing to increase the frame rate. Moreover, the staggered pattern (Figure 1b) results in large transmit grating lobes. Side lobes appear in the receiver's beam profile in all the three designs at +5 and -5 degrees, with levels around -10dB. The large hole in the receive aperture of Figure 1c results in larger side lobes, which can be analysed by plotting the point-spread-function (PSF). The PSF of the current receiver was compared with the PSF of a fully populated 32 × 32 receiver, as shown in supplementary Figure 3. The transfer function of the individual elements was obtained from the PZ-Flex simulations. The comparison of the two PSFs shows only a small difference in the way a single point is imaged by the receiver. We have chosen the design with central transmitter (Figure 1c) because of its lower level of grating lobes and excellent lateral resolution resulting in a PSF almost as good as a fully populated receiver array of the same size (supplementary Figure 3).

Prototyping

Figure 2 depicts the schematic of a miniature 3D TEE probe and a photograph of our matrix transducer prototype with a front-end ASIC. The layout of our central transmitter design and a schematic showing the concept of micro-beamforming in the receive sub-groups is depicted in Figure 2b and 2c. Note that two rows and columns of elements in the receive part (the dark grey 'cross') had to be sacrificed to allow for access to the 64 central transmit elements via the metal interconnect layers. Figure 2d is depicting the details of the various layers, described above, for manufacturing the prototype.
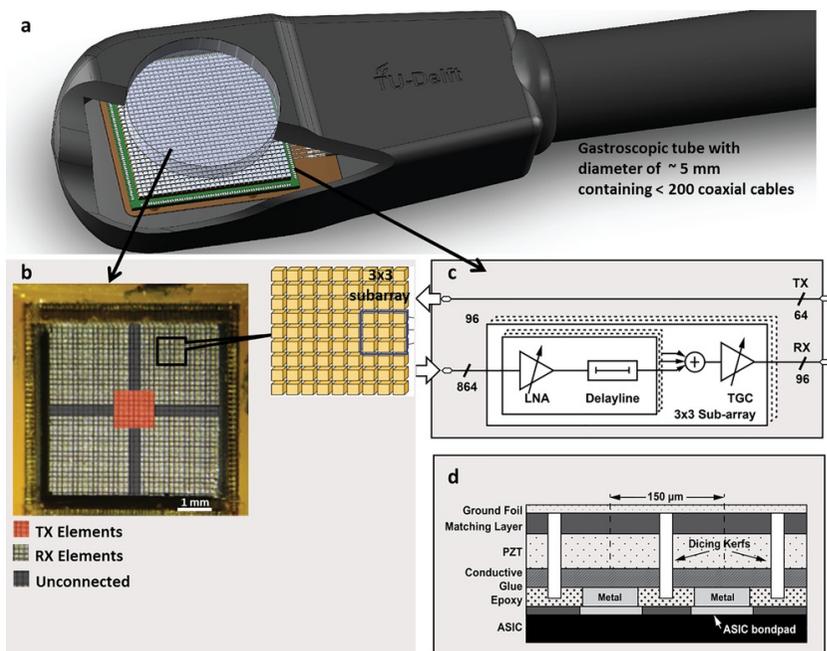

Fig.2 a) A schematic of a miniature 3D TEE probe with front-end ASIC; b) The layout of our prototype for pediatric 3D TEE transducer; c) The concept of the micro-beamforming in the ASIC; d) The detailed cross section of various layers of the prototype transducer with total thickness of 683 μm (not to scale).

alt-text: Fig 2

Acoustic characterization

The variation in the sensitivity of transmitters (individual elements) and receivers (individual sub-groups) of the prototype are depicted in Figure 3. There were two sub-groups among the receivers and one single element among the transmit elements with no signals (dark blue) which were excluded from the sensitivity variation measurements. The area in the middle of Figure 3a corresponds to the transmit part of the array. The sensitivity variation of the transmit array was measured separately and displayed in Figure 3b. The sub-groups of the receivers show a sensitivity variation of 7.6dB and individual elements of the transmitter have a sensitivity variation range less than 1dB.
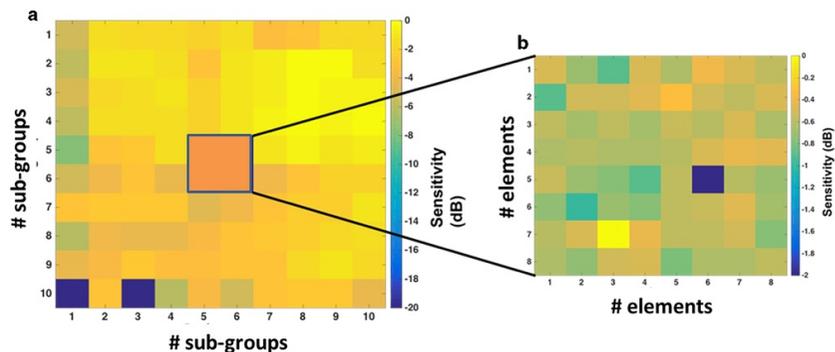
Fig.3 a) Sensitivity variation of the receive sub-groups of the prototype. The dark blue square in the centre shows the transmit sub-array. b) Sensitivity variation of each individual element (8 × 8) of the transmit sub-array.

alt-text: Fig 3

The transfer functions of three single elements of the transmit array of the prototype are plotted in Figure 4. The slight time shift in the time signals corresponds to the different locations of the elements with respect to the hydrophone. The Fourier transforms of the signals (Figure 4b) show a mean centre frequency of 5.8MHz with a mean -6dB bandwidth of 67%.
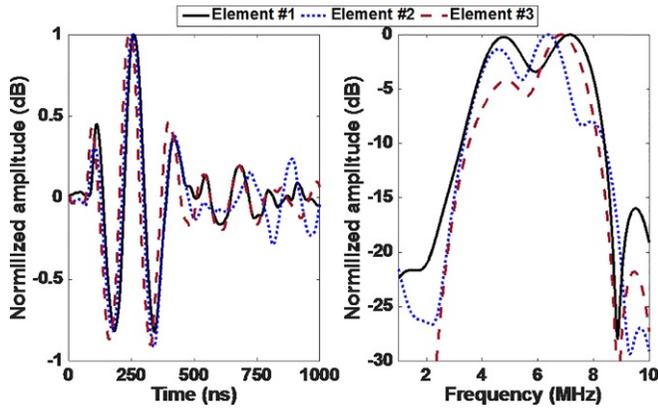

Fig.4 Transmit transfer function of three randomly selected single elements of the prototype transmit sub-array in a) time domain and b) frequency domain.

alt-text: Fig 4

The peak-to-peak output pressure recorded by the needle hydrophone at 30mm from the transducer surface as a function of the peak-to-peak input voltage is plotted in supplementary Figure 4. The efficiency of the transmit array (8 × 8 elements) is calculated to be around 6kPa/V at the distance of 30mm.

The result of the pulse-echo measurements is shown in Figure 5 where the received echo signals from the quartz plate of three different sub-groups are plotted in time and frequency domain. The amplitudes of the time signals in Figure 6a are displayed in arbitrary units. The normalized Fourier transforms of these time signals are shown in Figure 5b. The slight time shift observed in the time signals is due to the different locations of these sub-groups.
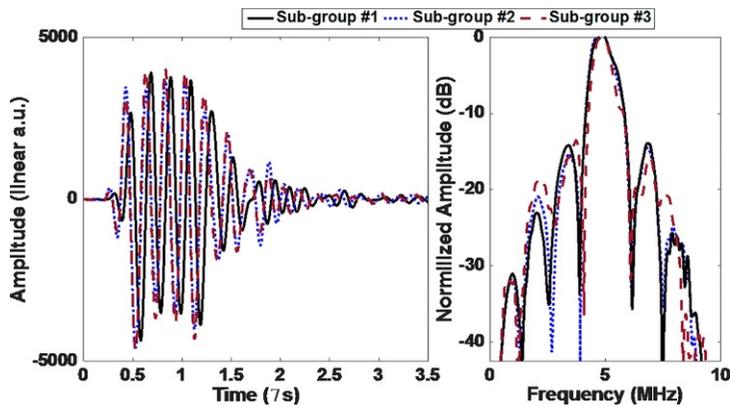

Fig.5 Received echo signals by three different sub-groups from a quartz plate 5mm away from the surface of the transducer in a) time domain and b) frequency domain.
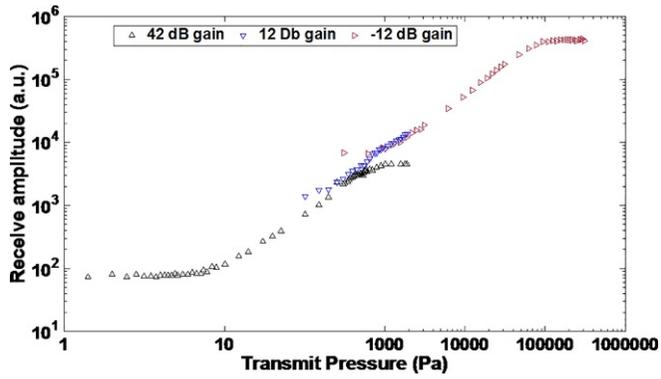
alt-text: Fig 5

Fig. 6 Measured peak-to-peak signal amplitude recorded by the Verasonics as a function of the peak-to-peak pressure at the surface of the transducer array for three different gain settings.

alt-text: Fig 6

The acoustic dynamic range of the prototype is plotted in Figure 6. The lowest detectable pressure is 5 Pa. This pressure was measured when the ASIC gain was set to 42dB. The highest detectable pressure before saturation of the signal is 84 kPa, which was measured when the ASIC gain was set to -12dB, resulting in an acoustic dynamic range of 85dB (5 Pa to 84 kPa) for this prototype.

The transmit-receive beam profile for the lateral and elevation direction and three different steering angles of (0°,0°), (17°,17°), and (37°,37°) are shown in Figure 7. In this Figure, the normalised peak-to-peak received pressure is plotted as a function of angle for each steering setting. The plot shows that the -6dB opening angle of the transmit-receive array is about 4°, and that the transmitter and receiver sub-groups can be steered effectively to any of the three angles (0°, 17°, and 37°) in both lateral and elevation directions.
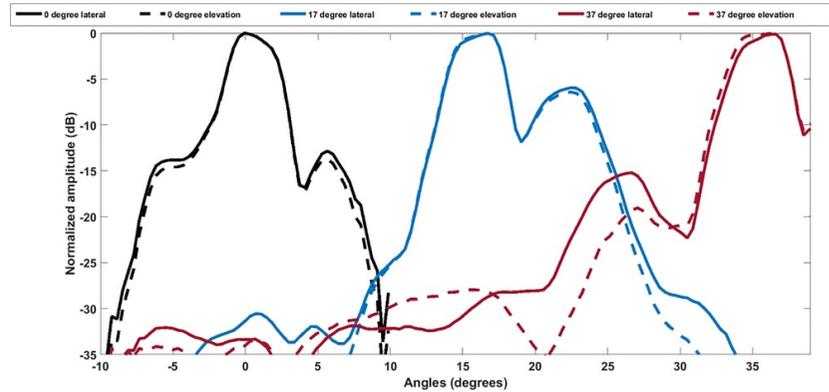
Fig.7 Transmit-receive beam profile of the prototype in lateral and elevation directions for three different steering angles ((0°,0°), (17°,17°), and (37°,37°)).

alt-text: Fig 7

3D Imaging

Figure 8a shows the positions of the 5 point scatterers (5 steel balls on needles) of the phantom, and Figure 8b shows the corresponding volume rendered image of this phantom placed on a c-plane at 40mm with 40dB dynamic range. In the rendered image, the positions of the point scatterers accurately matched with the actual positions of the scatterers. For each scatterer, one main lobe and four side lobes (in both lateral and elevation directions) are observed.

Fig.8 a) Pattern of 5 point scatterers (5 steel balls on needles). b) volume-rendered 3-D image with 40dB dynamic range.
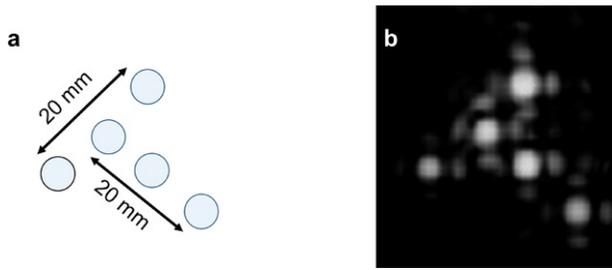
alt-text: Fig 8

Discussion

A front-end ASIC with an integrated 32 × 32 PZT matrix transducer has been designed and fabricated to enable next generation miniature ultrasound probes for real-time 3D TEE. The transducer array is split into a transmit sub-array and receive sub-groups. To address the critical challenge of cable count reduction, sub-array receive beamforming is realized in the ASIC with a highly compact and power-efficient circuit-level implementation, which utilizes the mismatch-scrambling technique to optimize the dynamic range. A power- and area-efficient LNA architecture is proposed to further optimize the performance. Based on these features, the ASIC demonstrates state-of-the-art power and area efficiency, and has been successfully applied in 3D ultrasound imaging.

The details of the ASIC design and its performance have been reported in our earlier publications (Chen, et al. 2017). The functionality of the ASIC was tested in a proof of concept study where a 9 × 12 array with a larger pitch of 200µm was fabricated on top of the ASIC for basic acoustic measurements. The receive ASIC integrates both the front-end signal conditioning circuits and the micro-beamformer. In this prototype, the signal conditioning circuit has a triple-level LNA and a quad-level TGC amplifier providing a total programmable gain range of 54dB.

An important feature of a TEE probe which should meet the FDA regulations is low in-probe power dissipation to prevent excessive tissue temperature rise. Such requirements apply to both the largest transmit power and the self-heating associated with the in-probe electronics. According to the regulations, the maximum temperature that may be attained by the surface is restricted to 41 degrees Celsius. This limits the total power budget of the in-probe transmit and receive circuit to about 0.5W (Yu 2012). The state-of-art of ultrasound front-end ASICs has a power consumption of a few mW per channel, adding up to several Watts for the entire array (Bhuyan, et al. 2013, Wygant, et al. 2008). In our design the 64 (8 × 8) transmitter sub-array in the center is electrically separated from the receive electronics. This configuration allows the use of dense low-voltage IC technology for the ASIC, thus saving power and area. Our ASIC design consumes only 0.27 mW per element, adding up to 230 mW for the entire array in full receive operation (Chen, et al. 2016). Our transmitter dissipates 267 mW in a worst case scenario of real-time imaging (64 elements, 5kHz prf, 5 cycles, 3kohm real impedance, pulse amplitude 50V RMS), which make the total dissipation less than 0.5 Watt. The lack of transmit electronics and the relatively small transmit aperture also limit the transmit heat generation with respect to other devices (Chen, et al. 2014). Also, despite the missing elements in the receive aperture, our numerical study shows that the PSF limiting the resolution in the image of our probe is comparable with a fully populated receiver probe of the same dimensions. Our design, compared to (Bhuyan, et al. 2013) which uses the majority of elements to transmit and a sparse array to receive, achieves better receiving sensitivity and lower side-lobes.

The sensitivity variation range between the elements was found to be 0.97dB for the transmit sub-array and 7.6dB for the receive array, confirming the quality of the fabrication process. The higher sensitivity variations observed in our measurements is partly due to the incident beam of the single element transducer used as an external excitation which has about 2dB variation over the 5mm size of the receive aperture of the prototype. Moreover, the elements at the edges of the probe are also more prone to mechanical damages during the manufacturing process increasing the variation range.

The transfer function of the single elements of the prototype shows a centre frequency of 5.8MHz and a fractional bandwidth of 67%. The reverberation signals that appear after the main signal in the time trace are caused by reflections from a thin foil which acts as an acoustic window to the water tank. The foil was not perfectly flat, and the transit time in the acoustic coupling gel between the probe and foil varied for different elements. This difference was observed in the different reverberation times in the time traces, and corresponding differences in dip-locations in the transfer functions. As such, this artefact is caused by the measurement setup, not by the probe itself.

The array has been mounted on top of an ASIC in order to reduce the electric signal losses that would otherwise occur between the acoustic stack and the mainframe. However, the silicon layer of the ASIC (300 µm) has a very low acoustic attenuation, and can sustain travelling lateral waves with a shear component. By exciting an element, such waves will be generated in the silicon layer, and these will transport a portion of the acoustic energy into the neighbouring elements or even into the element itself, when the wave is reflected back from the edges of the silicon layer. This mechanism effectively leads to acoustical cross-talk between the elements inthe matrix array degrading

the beam profile (Shabanimotlagh, et al. 2017). Similar problems have been reported in capacitive micromachined ultrasound transducers (CMUT) where the silicon substrate induces significant acoustic crosstalk between array elements (Xuecheng, et al. 2001). Although some compensation signal processing for such crosstalk has been proposed in the CMUT field (Shiwei, et al. 2003, Zhou and Hossack 2007), a more practical solution to the problem is to optimize the manufacturing process. Two methods have been proposed recently (Shabanimotlagh, et al. 2017): 1) Reducing the thickness of the silicon layer and adding an absorbing backing layer; 2) dicing the back side of the silicon layer underneath the ASIC. Although the effect of silicon (as an imperfect backing layer) on the acoustic stack has been partially addressed within our optimization process, we have not included any effects that lateral modes induced in the silicon layer might have on our array. We anticipate that reducing the thickness of the silicon layer and adding an absorbing backing layer will not only diminish the cross-talk but will also improve the bandwidth of the transducer.

The programmable gain settings of the LNA and the TGC signal conditioning circuit of the ASIC provide a total gain range of 54dB, which results in the large overall acoustic dynamic receive range of 85dB for our prototype. Thanks to this large receive dynamic range, small echo signals (as low as 5 Pa) can be detected by the receivers. Also, in our design, the separation of the transmit array from the low voltage receive electronics enables the transmit elements to be driven by high input voltages. The transmit efficiency of 6kPa/V of the transmit array guarantees that a sufficiently large pressure (e.g. 600 kPa with an input voltage of 100 V) can be generated by the transmitters.

While the transmit sub-array of the prototype can be steered to any angle up to ±45°in both lateral and elevation directions, the receive sub-groups are designed to be pre-steered at five different angles in both lateral and elevation directions: 0°, ±17°, and ±37°; i.e., to 25 fixed angles in 3D space. The overall transmit-receive steering is successfully demonstrated for these angles and the opening angle of the overall beam profile is about 4°. The beam width of the single presteered receive groups is wide enough (44°) to support beamforming of many such beams within the overlap of transmit and receive. Hence, for a transmit-receive event steered to a certain angle, only a specific sub-volume around that angle was beamformed. Despite of the receive grating lobes due to the sub-array pitch, the narrow opening angle of the transmit-receive beam guarantees significant reduction of the grating lobes in the final 3D image if an appropriate transmit-receive event is applied.

Our prototype with on-board micro-beamforming and a small central transmitter allows for multiline parallel beamforming at high framerate with a low number of channels within the limitations of the small aperture size of the transducer. Because of the architecture of our probe, existing 3D parallel beamforming techniques (Shattuck, et al. 1984, Hergum, et al. 2007, Tong, et al. 2014, Hasegawa, et al. 2011) were not suitable. Therefore, novel multiline 3D beamforming approaches were proposed that utilize the capabilities of the prototype transducer to produce volumes at high frame rate with good image quality (Bera, et al. 2018). Results indicate that the proposed multiline 3D beamforming techniques with the prototype matrix transducer can produce volumes with good image quality at a maximum rate of 300Hz, suitable for real-time paediatric 3D TEE. In simulation, the width of point spread functions, lateral shift invariance and clutter level were similar to those using conventional single line acquisitions with a hypothetical, idealized matrix transducer of the same size. Our proposed method can produce volumes with -6dB main lobe widths of ~4° and side lobe levels lower than −20dB, with a total opening angle of 90° × 90°.

Currently our prototype is mounted on a large PCB for acoustic characterization and therefore it is not suitable for (pre-)clinical use yet. In future work, a prototype of the probe will be assembled on the tip of a gastroscopic tube for (pre-)clinical validation.

Conclusion

In this article we have described the acoustic design, fabrication and characteristics of a PZT on CMOS 3D-TEE transducer capable of real-time 3D imaging. We have optimized the acoustic stack using finite element modeling (PZFlex). The 8 × 8 transmit sub-array has a transmit efficiency of 6kPa/V at 30mm and the single elements have a centre frequency of 5.8MHz and a –6dB fractional bandwidth of 67%. The receive dynamic range is 85dB with minimum and maximum detectable pressures of 5 Pa and 84 kPa. The micro-beamforming circuits within the ASIC effectively reduce the receive channel count to 96 receive lines, and the functionality of the sub-groups has been illustrated. The combined transmit-receive beams are successfully steered to the 25 pre-defined angles in 3D space to enable real-time 3D TEE with proper transmit-receive strategies.

Uncited References

Diarra et al., 2016, Hasegawa and Kanai, 2011 Jul 1, ONDA 2017, Bhuyan et al., 2013

Acknowledgements

Supplementary materials

Supplementary material associated with this article can be found, in the online version, at doi:10.1016/j.ultrasmedbio.2018.06.009.

References

Abboud NN, Wojcik GL, Vaughan DK, Mould J, Powell DJ and Lisa N, Electromechanical modeling using explicit time-domain finite elements, In: *1993 Proceedings IEEE Ultrasonics Symposium, 1107-12 vol.2,* 1993.

Austeng A and Holm S, Sparse 2-D arrays for 3-D phased array imaging - design methods, *IEEE Transactions on Ultrasonics, Ferroelectrics, and Frequency Control* **49**, 2002, 1073–1086.

Bera D, Raghunathan SB, Chen C, Chen Z, Pertijs MA, Verweij MD, Daeichin V, Vos HJ, van der Steen AF, de Jong N and Bosch JG, Multiline 3D beamforming using micro-beamformed datasets for pediatric transesophageal echocardiography, *Physics in Medicine & Biology* **63** (7), 2018, 075015.

Bhuyan A, Choe JW, Lee BC, Wygant I, Nikoozadeh A, Oralkan O and Khuri-Yakub BT, 3D volumetric ultrasound imaging with a 32x32 CMUT array integrated with front-end ICs using flip-chip bonding technology, *2013 IEEE International Solid-State Circuits Conference Digest of Technical Papers* 2013, 396–397.

Bhuyan A, Choe JW, Lee BC, Wygant IO, Nikoozadeh A, Ö O and Khuri-Yakub BT, Integrated Circuits for Volumetric Ultrasound Imaging With 2-D CMUT Arrays, *IEEE Transactions on Biomedical Circuits and Systems* **7**, 2013, 796–804.

Blaak S, Lancée CT, Bosch JG, Prins C, AFWvd Steen and Nd Jong, A matrix transducer for 3D Transesophageal Echocardiography with a separate transmit and receive sub-array, *2011 IEEE International Ultrasonics Symposium* 2011, 2341–2344.

Chen C, Chen Z, Bera D, Raghunathan SB, Shabanimotlagh M, Noothout E, Chang ZY, Ponte J, Prins C, Vos HJ and Bosch JG, A Front-End ASIC With Receive Sub-array Beamforming Integrated With a 32 × 32 PZT Matrix Transducer for 3-D Transesophageal Echocardiography, *IEEE Journal of Solid-State Circuits* **52** (4), 2017, 994–1006.

Chen C, Raghunathan SB, Yu Z, Shabanimotlagh M, Chen Z, Zy Chang, Blaak S, Prins C, Ponte J, Noothout E, Vos HJ, Bosch JG, Verweij MD, Nd Jong and Pertijs MAP, A Prototype PZT Matrix Transducer With Low-Power Integrated Receive ASIC for 3-D Transesophageal Echocardiography, *IEEE Transactions on Ultrasonics, Ferroelectrics, and Frequency Control* **63**, 2016, 47–59.

Chen K, Hae-Seung L and Sodini CG, A Column-Row-Parallel ASIC architecture for 3D wearable / portable medical ultrasonic imaging, *2014 Symposium on VLSI Circuits Digest of Technical Papers* 2014, 1–2.

Christiansen TL, Rasmussen MF, Bagge JP, Moesner LN, Jensen JA and Thomsen EV, 3-D imaging using row-column-addressed arrays with integrated apodization- part ii: transducer fabrication and experimental results, *IEEE transactions on ultrasonics, ferroelectrics, and frequency control* **62**, 2015, 959–971.

Cobbold RSC. Foundations of Biomedical Ultrasound, 2006.

Diarra B, Liebgott H, Robini M, Tortoli P and Cachard C, Novel strategies in 2D sparse arrays for 3D ultrasound imaging, *Physica Medica: European Journal of Medical Physics* **32**, 2016, 420–421.

Fisher R, Thomenius K, Wodnicki R, Thomas R, Cogan S, Hazard C, Lee W, Mills D, Khuri-Yakub B, Ergun A and Yaralioglu G, Reconfigurable arrays for portable ultrasound, *IEEE Ultrasonics Symposium* **200**, 2005, 495–499.

Gopal AS, Keller AM, Shen Z, Sapin PM, Schroeder KM, King DL, Jr. and King DL, Three-dimensional echocardiography: in vitro and in vivo validation of left ventricular mass and comparison with conventional echocardiographic methods, *J Am Coll Cardiol* **24**, 1994, 504–513.

Handke M, Schäfer DM, Heinrichs G, Magosaki E and Geibel A, Quantitative Assessment of Aortic Stenosis by Three-Dimensional Anyplane and Three-Dimensional Volume-Rendered Echocardiography, *Echocardiography* **19** 2002, 45–53.

Hasegawa H and Kanai H, High-frame-rate echocardiography using diverging transmit beams and parallel receive beamforming, *Journal of medical ultrasonics* **38** (3), 2011 Jul 1, 129–140.

Hergum T, Bjastad T, Kristoffersen K and Torp H, Parallel beamforming using synthetic transmit beams, *IEEE transactions on ultrasonics, ferroelectrics, and frequency control* **54** (2), 2007 Feb, 271–280.

Jensen JA., Field: A program for simulating ultrasound systems, In: *10th Nordicbaltic Conference on Biomedical Imaging, Vol. 4, Supplement 1, Part 1: 351–353,* 1996.

Kortbek J, Jensen JA and Gammelmark KL, Sequential beamforming for synthetic aperture imaging, *Ultrasonics* **53**, 2013, 1–16.

Kwak J, Andrawes M, Garvin S and D'Ambra MN, 3D transesophageal echocardiography: a review of recent literature 2007–2009, *Current Opinion in Anesthesiology* **23**, 2010, 80–88.

Light ED, Idriss SF, Wolf PD and Smith SW, Real-time three-dimensional intracardiac echocardiography, *Ultrasound in Medicine & Biology* **27**, 2001, 1177–1183.

Logan AS, Wong LL, Chen AI and Yeow JT, A 32 x 32 element row-column addressed capacitive micromachined ultrasonic transducer, *IEEE Trans Ultrason Ferroelectr Freq Control* **58**, 2011, 1266–1271.

Matrone G, Savoia AS, Terenzi M, Caliano G, Quaglia F and Magenes G, A volumetric CMUT-based ultrasound imaging system simulator with integrated reception and μ-beamforming electronics models, *IEEE Transactions on Ultrasonics, Ferroelectrics, and Frequency Control* **61**, 2014, 792–804.

ONDA, How can I estimate the hydrophone directivity? (1290 Hammerwood, Sunnyvale, CA 94089, USA), http://ondacorp.com/tecref_faqs.shtml, 2017.

Pandian NG, Hsu T-L, Schwartz SL, Weintraub A, Cao Q-L, Schneider AT, Gordon G, England M and Simonetti J, Multiplane Transesophageal Echocardiography, *Echocardiography* **9**, 1992, 649–666.

Provost J, Papadacci C, Arango JE, Imbault M, Fink M, Gennisson JL, Tanter M and Pernot M, 3D ultrafast ultrasound imaging in vivo, *Physics in medicine and biology* **59**, 2014, L1–l13.

Raichlen JS, Trivedi SS, Herman GT, John Sutton MGS and Reicher N, Dynamic three-dimensional reconstruction of the left ventricle from two-dimensional echocardiograms, *Journal of the American College of Cardiology* **8**, 1986, 364–370.

Roelandt JR, Thomson IR, Vletter WB, Brommersma P, Bom N and Linker DT, Multiplane transesophageal echocardiography: latest evolution in an imaging revolution, *J Am Soc Echocardiogr* **5**, 1992, 361–367.

Roux E, Ramalli A, Liebgott H, Cachard C, Robini MC and Tortoli P, Wideband 2-D Array Design Optimization With Fabrication Constraints for 3-D US Imaging, *IEEE transactions on ultrasonics, ferroelectrics, and frequency control* **64**, 2017, 108–125.

Roux E, Ramalli A, Tortoli P, Cachard C, Robini M and Liebgott H, 2D Ultrasound Sparse Arrays Multi-Depth Radiation Optimization Using Simulated Annealing and Spiral-Array Inspired Energy Functions, *IEEE Trans Ultrason Ferroelectr Freq Control* 2016.

Salustri A, Spitaels S, McGhie J, Vletter W and Roelandt JRTC, Transthoracic three-dimensional echocardiography in adult patients with congenital heart disease, *Journal of the American College of Cardiology* **26**, 1995, 759–767.

Sapin PM, Schroeder KD, Smith MD, DeMaria AN and King DL, Three-dimensional echocardiographic measurement of left ventricular volume in vitro: Comparison with two-dimensional echocardiography and cineventriculography, *Journal of the American College of Cardiology* **22**, 1993, 1530–1537.

Savord B and Solomon R, Fully sampled matrix transducer for real time 3D ultrasonic imaging, *IEEE Symposium on Ultrasonics, 2003* **1**, 2003, 945–953, Vol.1.

Seward JB, Khandheria BK, Oh JK, Abel MD, Hughes Jr RW, Edwards WD, Nichols BA, Freeman WK and Tajik AJ, Transesophageal Echocardiography: Technique, Anatomic Correlations, Implementation, and Clinical Applications, *Mayo Clinic Proceedings* **63**, 1988, 649–680.

Shabanimotlagh M, Daeichin V, Raghunathan SB, Kruizinga P, Vos HJ, Bosch JG, Pertijs M, Jong Nd and Verweij M, Optimizing the directivity of piezoelectric matrix transducer elements mounted on an ASIC, *2017 IEEE International Ultrasonics Symposium (IUS)* 2017, 1–4.

Shattuck DP, Weinshenker MD, Smith SW and von Ramm OT, Explososcan: A parallel processing technique for high speed ultrasound imaging with linear phased arrays, *The Journal of the Acoustical Society of America* **75** (4), 1984 Apr, 1273–1282.

Shell RR. 2002 Three-dimensional imaging system for sonar system: Google Patents.

Shiwei Z, Wojcik GL and Hossack JA, An approach for reducing adjacent element crosstalk in ultrasound arrays, *IEEE Transactions on Ultrasonics, Ferroelectrics, and Frequency Control* **50**, 2003, 1752–1761.

Sugeng L, Weinert L, Thiele K and Lang RM, Real-time three-dimensional echocardiography using a novel matrix array transducer, *Echocardiography* **20**, 2003, 623–635.

Tong L, Ramalli A, Jasaityte R, Tortoli P and D'hooge J, Multi-transmit beam forming for fast cardiac imaging—Experimental validation and in vivo application, *IEEE transactions on medical imaging* **33** (6), 2014 Jun, 1205–1219.

Wygant IO, Jamal NS, Lee HJ, Nikoozadeh A, Oralkan O, Karaman M and Khuri-yakub BT, An integrated circuit with transmit beamforming flip-chip bonded to a 2-D CMUT array for 3-D ultrasound imaging, *IEEE transactions on ultrasonics, ferroelectrics, and frequency control* **56**, 2009, 2145–2156.

Wygant IO, Zhuang X, Yeh DT, Oralkan O, Ergun AS, Karaman M and Khuri-yakub BT, Integration of 2D CMUT arrays with front-end electronics for volumetric ultrasound imaging, *IEEE Transactions on Ultrasonics, Ferroelectrics, and Frequency Control* **55**, 2008, 327–342.

Xuecheng J, Oralkan O, Degertekin FL and Khuri-Yakub BT, Characterization of one-dimensional capacitive micromachined ultrasonic immersion transducer arrays, *IEEE Transactions on Ultrasonics, Ferroelectrics, and Frequency Control* **48**, 2001, 750–760.

Yu Z, Doctoral thesis, 2012.

Zhou S and Hossack JA, Reducing inter-element acoustic crosstalk in capacitive micromachined ultrasound transducers, *IEEE Transactions on Ultrasonics, Ferroelectrics, and Frequency Control* **54**, 2007, 1217–1228.

Appendix. Supplementary materials

Multimedia Component 1

alt-text: Image, application 1

Queries and Answers

Query: Please confirm that givennames and surnames have been identified correctly.
Answer: for the third author Maysam is givvenname and Shabani Motlagh is surname

Query: Please check correctness of short running title.
Answer: Correct

Query: This section comprises references that occur in the reference list but not in the body of the text. Please position each reference in the text or, alternatively, delete it.
Answer: The only uncited reference is deleted